JOURNAL OF COMPUTATIONAL PHYSICS 102, 1–17 (1992)

REVIEW ARTICLE

Numerical Modeling of Macro and Micro Behaviors of Materials in Processing: A Review

A. A. TSENG AND J. ZOU

Department of Mechanical Engineering and Mechanics, Drexel University, Philadelphia, Pennsylvania 19104

H. P. WANG

General Electric R & D, Schenectady, New York 12301

AND

S. R. H. HOOLE

Harvey Mudd College, Claremont, California 91711

Received August 30, 1990; revised June 20, 1991

Numerical techniques used for modeling the macroscopic and microscopic behavior of materials in processing are reviewed. The macromodels are based on the concept of a material continuum for which the densities of mass, momentum, and energy exist in the mathematical sense of the continuum and the microstructure of matter can be ignored. The micromodels, on the other hand, are based on the concepts of micromechanics and statistics applied to the study of the microstructure of the material. In this paper, formulation of the partial differential equations that govern the macroscopic behavior of materials resulting from the material continuum assumption is first presented. The relevant numerical techniques for solving these equations and for handling the associated boundary conditions are then discussed. As a demonstration, a continuous drawing process is modeled to illustrate the procedure involved and the information revealed. In microscopic modeling, the numerical and statistical techniques used to simulate the microstructure formation of materials are reviewed. Examples applied to solidification and recrystallization as well as defect formation are then presented. Finally following an examination of the approaches that incorporate the microscopic models into the macroscopic models, recommendations on the future development are given.

1. INTRODUCTION

Numerical techniques have been extensively utilized for modeling the macroscopic and microscopic behaviors of materials in processing in the past two decades. In macroscopic modeling, the concept of material continuum for which the densities of mass, momentum, and energy exist in the mathematical sense of the continuum is applied to study the physical behavior of materials. The continuum is a mathematical idealization of the real world and is applicable to problems in which the microstructure of matter can be ignored. When the microstructure is to be studied, the concepts of micromechanics and statistics should be applied.

Based on either the continuum or micromechanics concept, partial differential equations governing different material behaviors can usually be formulated. It is well known that in macromodeling, the Navier–Stokes equation for the momentum field, the Fourier equation for the temperature field, and the Maxwell equation for the electromagnetic field [1, 2] are the respective governing equations. In general, these partial differential equations should be considered simultaneously. Consequently, depending on the stiffness of the system, advanced numerical coupling techniques which further complicate the already formidable situation are often required. For example, in modeling the induction heating process, the electromagnetic, heat transfer, and fluid flow behaviors are strongly coupled and should be solved together.

Many numerical techniques, including the finite difference method (FDM), finite element method (FEM), and boundary element method (BEM), have been developed to solve these differential equations with complex boundary conditions arising from material processing. Recently, the generalized finite difference method (GFDM) developed from the body-fitted concept has received great attention because of its inherent simplicity and flexibility in applica-

0021-9991/92 $5.00

tions to irregular geometry problems. It should be noted that this method requires some advanced mathematical skills [1, 2].

The boundary condition is a critical parameter for obtaining the final result. It is extremely difficult to determine or control the boundary conditions for the materials under processing. Recently, many numerical schemes have been developed to model the boundary conditions, particularly, the free and moving boundary problems through the finite element or finite difference methods. For the free boundary problem, Simpson's rule, the Galerkin finite element formulation approach, and the Lagrangian finite element formulation have usually been adopted. For the moving boundary problem, the volume of fluid technique using fixed meshes and the remeshing technique through an arbitrary Lagrangian–Eulerian formulation have been adapted.

After extensive development of macroscopic models, microscopic mathematical models have emerged in the last decade. These microscopic models attempt to describe quantitatively diverse phenomena occurring at the microstructure scale such as solidification, recrystallization, and defect formation. These phenomena include nucleation, growth, and impingement of grains. The micromodels are initially developed using a combination of basic theory and experimental observation. For more complex situations, numerical methods associated with a statistical approach such as the Monte Carlo method are applied to the microsopic modeling. Because the micromodels exhibit high nonlinearity, more restrictive numerical conditions, such as a smaller time step and a finer mesh size are often required for obtaining stable and convergent numerical solutions.

In this paper, following a discussion of the modeling aspects of the macro and micro behavior of materials, formulation of the governing partial differential equations for the macroscopic models are first reviewed. Then the principal numerical methods for solving these governing equations are discussed. The associated boundary conditions including the free and moving boundaries are also examined. To illustrate the modeling procedure involved, a continuous drawing process widely used in industry is considered. In microscopic modeling, the computational aspects of simulating the phenomena occurring at microstructure scales such as solidification, recrystallization, and defect formation are presented. The concept of coupling of the macro/microscopic modeling and its applications are also discussed with an illustration included. Finally, comments on future trends in modeling schemes are given.

II. MODELING OF MACROSCOPIC BEHAVIOR

Based on the concept of a material continuum, the formulation of the macro behavior of materials under processing is presented in this section.

Material Flow in Processing

Material processing involves flow through complex geometrical shapes and often includes free- or moving-surface flows; the flow properties are usually temperature dependent. Modeling of the material flow has to cope with these geometric and material non-linearities. In this subsection, formulation of material flow is considered.

Governing equations. A dynamic equation describing fluid motion may be obtained by applying Newton's second law to a field description of fluid flow in which the properties of a flow field are defined by continuous functions of space coordinates and time. The field description for fluid particles, in Cartesian tensor notation, is governed by:

$$\frac{\partial(\rho u_i)}{\partial t}+\frac{\partial(\rho u_i u_j)}{\partial x_j}=\rho b_i+\frac{\partial \sigma_{ji}}{\partial x_j} \tag{1}$$

and

$$\frac{\partial \rho}{\partial t}+\frac{\partial(\rho u_j)}{\partial x_j}=0, \tag{2}$$

where ρ is the density of the material melt; t is the time; x_j are the Cartesian coordinates; u_j is the velocity vector; b_i is the body force; and σ_{ji} is the stress tensor.

Constitutive equations. Before the momentum equations can be employed in the solution of problems, suitable expressions for the stresses, σ_{ij} in Eq. (1), must be obtained. For material melts, the constitutive relationships may be obtained using either the continuum mechanics approach or the molecular approach. The popular Newtonian fluid or the well-known power law model is usually developed through the continuum mechanics approach. There are many other consitutive relationships used for different material fluids. Some discusions on other non-linear constitutive equations may be found in Refs. [3, 4].

Primitive variable formulation. If the viscosity is non-Newtonian, the primitive variable approach is more convenient. The momentum equations can be solved in terms of the primitive variables, u_i and pressure (or stresses), as indicated in Eqs. (1) and (2). These equations play a dominant role in modeling the materials in the liquid state, since they contain distributed force terms for velocity within the liquid phase. The body forces of interest here are the buoyancy body forces. Other driving forces include surface forces resulting from temperature gradient-induced differences in surface tension and variation of phase densities across the melt–freeze interface which enter only as boundary conditions. These equations are only needed to describe the materials in the liquid state. In the solid phase, the velocity is zero. To obtain the temperature information, the momentum equation should be coupled with the heat transfer equation which will be discussed in the next section.

There have been a large number of modeling efforts using the primitive variable approach. Some numerical algorithms, such as SIMPLE and SIMPLER [5], have been developed to solve these simultaneous primitive-variable equations. The SIMPLE algorithm is based on a successive guess-and-correct procedure. The velocity components are first calculated from the momentum equations using an assumed pressure field. The pressures and velocities are then corrected so as to satisfy the continuity equation. This process continues until the solution converges. This iteration scheme has been successfully adopted in the conventional finite difference method as well as the generalized finite difference (GFD) method. The GFD method not only overcomes those difficulties arising from the non-uniform mesh arrangement but also maintains the inherent simplicity of the finite difference method. It has been adopted to model both the thermal [6] and flow [7] behaviors.

Vorticity variable approach. If the melt is Newtonian, the momentum equations can be solved either in terms of the primitive variables or indirectly in terms of the vorticities or stream functions. The concept of vorticity is very important for internal re-circulating flow. Mathematically, it is the curl of Eq. (1) that produces either buoyant or force stirring. The vorticity–velocity formulation could be used for the solution of the flow problem in the liquid metal. For three-dimensional problems, six dependent variables (three vorticity and three velocity components) need to be solved. This formulation avoids the necessity of a staggered-grid arrangement, which is required in the above primitive-variable approach [8], where difficulties are encountered with the pressure boundary conditions and instabilities resulting from satisfying continuity. Also the present formulation has better boundary conditions than the scalars/vector potential formulation [9]. In addition, although the stream function no longer exists in three-dimensional cases, the vorticity forms are useful for the interpretation of numerically predicted eddy strength, orientation, and direction of rotation in terms of the relative strength and orientation of the internally distributed driving forces within the liquid metal.

Mushy or transition state. In phase change problems, characterized by the mushy zone or the transition state, the governing equation, Eq. (1), should be modified to reflect the phase change. Ganesan and Poirier [10] recently used the volume-average technique to derive the momentum equation in the mushy zone during solidification. In order to avoid dealing with the complex interfacial geometry in the mushy zone at the microscopic scale, the microscopic equations were averaged over some representative elementary volume within the mushy zone (e.g., several dendrite arm spacings), while the macroscopic models can be resolved by standard techniques.

The average procedure is based on the continuum hypothesis that the average quantities should be continuous functions of space and time and should be independent of the size of the average volume. When the element volume is very small, the average mass density (liquid mass divided by total mass in one mesh) of the interdendritic fluid varies discontinuously. As the size of the element volume increases, the fluctuation of the average density diminishes till the density or other average quantities become independent of the size of element volume. If the size of the element volume continues to increase to a value larger than or closer to the size of the mushy zone, the average value of the liquid density will increase. Because the bulk liquid zone will be included in this element volume, a general momentum equation in the mushy zone can be written with the permeability of dendritic network:

$$
\begin{aligned}
&-f_1 \frac{\partial p}{\partial x_i} + \rho_1 f_1 g_i \\
&\quad + \frac{\partial}{\partial x_j}\left[\mu\left(\frac{\partial (f_1 u_i)}{\partial x_j} + \frac{\partial (f_1 u_j)}{\partial x_i}\right) - \frac{2\mu}{3}\delta_{ij}\frac{\partial (f_1 u_k)}{\partial x_k}\right] \\
&\quad - \mu\left[\frac{f_1^2}{K_{ij}} u_j + C_{ijk} u_k u_j\right] \\
&= \rho_1 f_1 \left[\frac{\partial u_i}{\partial t} + u_j \frac{\partial u_i}{\partial x_j}\right],
\end{aligned} \tag{3}
$$

where ρ_1 is density of the liquid, f_1 is volume fraction of the liquid, g_i is gravitational acceleration, u_i is mass average velocity of the interdendritic liquid, p is average pressure, μ is viscosity of the interdendritic liquid, C_{ijk} is third-order tensor resistance coefficient, and K_{ij} is permeability.

Heat Transfer in Material Processing

Heat transfer in material processing is complicated by the accompanying phase changes. The effective heat capacity formulation is utilized to reduce the number of governing equations for covering the liquid, solid, and mushy states of the material.

Governing equations. Normally, the end products are used in the solid phase, but most of the end-use properties and shapes are developed during fluid-state or solidification. Therefore, the heat transfer equation must be considered in the liquis, solid, and mushy phases. This leads to the enthalpy method being developed. The merit of this method is that a single equation can accommodate both the solid and liquid phases as well as the mushy state [11, 12]. The material temperature, T, can be predicted from

$$
\rho C_p^e \left(\frac{\partial T}{\partial t} + u_j \frac{\partial T}{\partial x_j}\right) = \frac{\partial}{\partial x_j}\left(k \frac{\partial T}{\partial x_j}\right) + \eta\phi, \tag{4}
$$

where k is the thermal conductivity, T is the temperature, u_j, the velocity, is directly computed from the momentum

equation, Eq. (1), and ϕ is the dissipation function, representing the internal heat generated by the viscosity dissipation which can be evaluated by providing the velocity distributions. The effective heat capacity C_p^e can be defined as

$$C_p^e = C_p + \frac{L}{T_l - T_s}, \qquad L = \begin{cases} L, & T_s \leqslant T \leqslant T_l \\ 0, & \text{otherwise,} \end{cases} \tag{5}$$

where C_p is the specific heat and L is the heat of fusion per volume. In the mushy region, the temperature is lower than the liquidus temperature, T_l, and higher than the solidus temperature, T_s. A linear relationship between the volume fraction of solid and T is assumed in the above equation. A similar assumption is also used for the thermal conductivity in the mushy region, k,

$$\frac{k - k_l}{k_s - k_l} = \frac{T_l - T}{T_l - T_s}, \tag{6}$$

where k_l and k_s are the conductivities at the liquidus and the solidus temperatures, respectively.

Heating Source-Electroheating

In material processing, heating is one of the major parameters in process operation and material property control. Many heating techniques have been developed including electromagnetic (or induction) heating, gas/oil fire heating, and electrical resistance radiant heating. While the latter two schemes can be simulated by imposing appropriate boundary conditions, the former one should be considered in the governing equation. As a result, the electromagnetic distribution has to be determined first. In this subsection, a formulation of the electromagnetic heating behavior is presented.

Electromagnetic equations. Electromagnetic behavior is governed by the Maxwell equations which, in their general forms, are coupled. For induction heating, the governing equations can be simplified to [12, 30]

$$\frac{\partial J_i}{\partial x_i} = 0 \tag{7}$$

$$\frac{\partial B_i}{\partial x_i} = 0 \tag{8}$$

$$e_{ijk} \frac{\partial E_k}{\partial x_j} = \frac{\partial B_i}{\partial t} \tag{9}$$

$$e_{ijk} \frac{\partial H_k}{\partial x_j} = J_i, \tag{10}$$

where J_i, B_i, E_i, and H_i are the current density, magnetic-flux density, electric-field intensity, and magnetic-field intensity, respectively; and e_{ijk} is the permutation symbol.

Constitutive equations. The associated constitutive equations are

$$B_i = \mu_m H_i \tag{11}$$

$$J_i = \sigma_e E_i, \tag{12}$$

where the material properties, μ_m and σ_e, are the magnetic permeability and the electric conductivity, respectively.

For the purpose of solution, the first-order differential equations involving both H_i and E_i are combined to give a second-order equation in H_i or E_i only. For the magnetic field intensity, the governing equation becomes

$$\frac{\partial^2 H_i}{\partial x_i^2} = \sigma_e \mu_m \frac{\partial H_i}{\partial t} - \frac{\partial}{\partial x_i}\left[H_i \left(\frac{1}{\mu_m} \frac{\partial \mu_m}{\partial x_i} \right) - \frac{1}{\sigma_e} \left(\frac{\partial \sigma_e}{\partial x_k} \frac{\partial H_k}{\partial x_i} - \frac{\partial \sigma_e}{\partial x_j} \frac{\partial H_i}{\partial x_j} \right) \right]. \tag{13}$$

Theoretically, with appropriate initial and boundary conditions, the above governing equations can be solved mathematically. However, as indicated by Tseng [12], it is a nontrivial task to describe the needed boundary or interface conditions in terms of those primary variables, such as H_i or B_i. As an alternative, it is convenient to use the magnetic vector potential A_i which is always continuous across the interface while H_i and B_i may not be so.

Magnetic vector potential formulation. The magnetic vector potential with nonlinear properties is often used to formulate the electromagnetic behavior. The adoption of the magnetic vector potential provides a more convenient form for handling the interface conditions and reducing the vector component. If translational or rotational symmetry exists, the magnetic vector potential may possess only one component.

Using the result of vector calculus, if $\partial B_i / \partial x_i = 0$ (Eq. 8) everywhere, there exists some vector field, A_i, and the corresponding governing equation can be found,

$$\frac{\partial^2 A_i}{\partial x_i^2} = \sigma_e \mu_m \left(\frac{\partial A_i}{\partial t} + \frac{\partial \varphi}{\partial x_i} \right) - \frac{1}{\mu_m} \left(\frac{\partial \mu_m}{\partial x_k} \frac{\partial A_k}{\partial x_i} - \frac{\partial \mu_m}{\partial x_j} \frac{\partial A_i}{\partial x_j} \right) \tag{14}$$

where φ is the electric scalar potential, or the simpler linear form, in terms of J_i,

$$\frac{\partial^2 A_i}{\partial x_j^2} = \sigma_e \mu_m \left(\frac{\partial A_i}{\partial t} + \frac{\partial \varphi}{\partial x_i} \right) = -\mu_m J_i. \tag{15}$$

For such fields, the above equation does not provide any particular advantage over the Poisson equation (13), since both are vector equations. However, as mentioned earlier, many circumstances occur, particularly where translational or rotational symmetry exists, in which J_i possesses only one vector component. In such cases, A_i may also possess only one component [30].

III. MODELING OF BOUNDARY CONDITIONS

Although the materials processing can be described by the above governing equations, it is still necessary to have or describe the associated boundary conditions for obtaining quantitative results by solving these equations. When the boundary is fixed and only the boundary conditions need to be evaluated, it is referred to as a "fixed boundary," e.g., the heat transfer at the interface. Otherwise, the boundary itself is unknown a priori and has to be determined and then used to estimate the dependent boundary conditions. When the boundary is in the steady state, this type of boundary is referred to as a "free boundary." Under the condition that the boundary changes due to kinematic and dynamic conditions, it is referred to as a "moving boundary."

The fixed boundary conditions are relatively straightforward and covered in many elementary numerical textbooks. The details of this condition, therefore, will not be discussed further in this section. Both free and moving surfaces are intrinsic characteristics of any shape-changing process. The development of efficient numerical techniques for tracking free and moving boundaries has been identified as one of the most challenging topics in process modeling research. In this section, modeling of the free and moving boundary conditions encountered in material processing will be discussed.

Free Boundary

Free boundary problems are defined as steady state problems involving free surfaces, and usually involve continuous forming processes such as extrusion, drawing, and calendering. Since the solution is a function of a surface shape which is not known a priori, the problem is a geometrically non-linear problem.

At the free surface, the three conditions are generally required: (1) zero normal velocity, (2) zero tangential stress, and (3) normal stress balanced by surface tension,

$$u_i n_i = 0 \tag{16a}$$

$$\sigma_{ij} n_j t_i = 0 \tag{16b}$$

$$\sigma_{ij} n_j n_i - S(1/\rho_1 + 1/\rho_2) = 0, \tag{16c}$$

where $u_i n_i$ is the velocity normal to the surface, $\sigma_{ij} n_j t_i$ is the stress component tangential to the free surface, $\sigma_{ij} n_j n_i$ is the normal stress, S is the surface tension coefficient, and ρ_1 and ρ_2 are the principal radii of curvature of the surface. If the boundary forces resulting from temperature gradient-induced differences in surface tension, e.g., the Manangoni effect, are included, the zero tangential stress condition, Eq. (16b), should be modified.

The contact line between a stationary solid wall and a flowing liquid is a static contact line. There are two types of static contact lines: those which remain at corners and those which are free to flow along with the wall. The boundary condition for the first type is the specified location of the contact line, whereas a contact angle is needed for the second type. For most extrusion/drawing types of processes the contact line remains at the die exit corner, and the first type of boundary condition is sufficient.

Kinematic boundary condition (iterative). The first successful solution for the free surface in die swell using the first surface conditions was due to Nickell *et al.* [13] through the finite element method. In the axisymmetric case, the radial coordinates at the free surface, $R(z)$, are integrated by the streamline equation, which is the equivalent form of Eq. (16a):

$$\frac{dR}{dz} = \frac{u_z[R(z), z]}{u_r[R(z), z]}. \tag{17}$$

With the numerical representation

$$R_{j+1}^{n+1} = R_j^{n+1} + \int_{z_j}^{z_{j+1}} \left[\frac{u_r}{u_z}\right]^n dz, \tag{18}$$

where the superscript n is the iteration number and the subscript j is the nodal position in the axial direction. The integral can be calculated using Simpson's rule. Chang *et al.* [14] also developed a similar approach using a more rigorous mathematical derivation.

Normal stress (iterative). For the case of small surface tension, the previous method, which updates the streamline coordinate with the newly calculated velocity vectors, i.e., the kinematic surface condition, is preferred. For larger surface tension, where the ratio of the surface tension to the viscous force becomes very large, the third boundary condition, which uses the normal stress equation for iteration, is needed because the kinematic technique does not converge [15, 16]. The relative importance between the viscous force and surface tension force can be described by the capillary number. The procedure using the third surface boundary condition for tracking the free surface is described in Refs. [17–19]. The basic concept here in successive approximations is to choose the surface condition which has a dominant effect on the surface shape for iterations.

Coupled finite element formulations. For problems within a range of intermediate surface tension effects, both iterative approaches converge very slowly. Ruschak [20] and Kistler and Scriven [15] indicated that the simultaneous calculation of the complete set of nonlinear equations for the free surface location and the field variables (velocity components and pressure) give better convergence than the successive approximations. This additional degree of freedom represents a free nodal position with respect to some reference point.

In this coupled approach the first surface condition, Eq. (16a), is posed in an integral form representing the absence of mass flow across the surface

$$\int_S n_i u_i \, dS := 0. \tag{19}$$

Following a Galerkin finite element formulation approach, the continuity equation, the momentum equation, and the above surface integral equation are used to form a system of nonlinear algebraic equations. These can be solved by Newton's method at a quadratic rate of convergence. The other two surface conditions, Eq. (16b) and Eq. (16c), are applied in the standard way for Galerkin weighted residual formulations [21].

Transient Lagrangian. Another effective approach is to use a Lagrangian description of fluid motion, including time as an independent variable [22]. In the Lagrangian formulation, the independent variables are the material particles and time, and the dependent variables are the spatial coordinates of all material particles and the time derivatives of the coordinates.

In the Lagrangian finite element formulation, the material (rather than the space) and time need to be discretized. The elements representing the discretized material then move with the newly calculated velocities during each time step. The prediction of free surface location is naturally included in this moving mesh algorithm. The first free surface condition, the zero normal velocity, will not be satisfied until a steady state is reached.

Uncoupled approaches are generally easier to implement and require less computer storage at the expense of slower convergence and a limited range of surface tension effects. In coupled approaches the solutions converge with a quadratic rate for a broad range of surface tension effects, but the program is more complicated. In the transient Lagrangian formulation, the free surface locations are naturally determined as the solution reaches its steady state.

Moving Boundary

In a moving boundary problem, part of the boundary moves according to prescribed kinematic and dynamic conditions. Moving boundary problems are usually associated with cyclic or batch type material processes, whereas free boundary problems are connected with continuous type processing.

Like the free boundary techniques, there are many algorithms for tracking moving boundaries depending upon the choice of numerical method (finite element, finite difference, or boundary element) and the selection of a meshing system (moving or fixed meshes). Using the fixed mesh approach, the resolution of the free flow front definition is in the order of the mesh size. In achieving a better free front definition, the moving mesh approach seems to have good potential.

Volume of fluid using fixed meshes. The volume of fluid (VOF) technique for front tracking, which was originally developed for the finite difference method [23–25], has been extended for for finite element applications. The VOF technique uses a fixed-mesh system with flow fronts passing through. Eliminating the remeshing requirement is the key benefit of using this fixed-mesh system for modeling moving boundary problems. The VOF algorithms for tracking the weldlines, where two flow fronts meet are much simpler than other techniques, such as adding elements or polynomial curve fitting. The triangle element is selected for its flexibility as well as its simplicity in integrating with this front tracking algorithm.

The VOF technique for defining the flow front is derived from the basic concept of mass conservation in a compressible flow. This very powerful concept for finite element applications is extended here. Since the finite element method deals with integral equations, the integral form of this VOF equation becomes

$$\int f \, u_n \, dA = \frac{\partial}{\partial t} \int f \, dV, \tag{20}$$

where f is the percentage of fill for each finite element control volume. This f parameter is defined as the "density" of the control volume.

For each filling time step, the percentage of fill for each control volume must be computed by using this "conservation of mass equation." During the calculation, the normal component of the velocity vector should be integrated along each segment of the control volume boundary. Just like the density calculation, the f function can be determined by dividing the total current mass by the total volume. The partially filled control volumes are defined as the flow fronts. If the computed f is 100%, the control volume is completely filled. Conversely, if f is zero, the control volume is empty. The filling analysis of the polymer injection molding process is one typical application of this VOF technique.

Remeshing techniques using an ALE formulation. The arbitrary Lagrangian–Eulerian (ALF) formulation has been found to be very effective for solving this type of moving free surface problem [24–28]. The conservation

equations for momentum and energy are reformulated to accommodate the moving mesh. The time derivatives for the velocities and the temperature become

$$\left.\frac{\partial u_i}{\partial t}\right|_M = \left.\frac{\partial u_i}{\partial x_j}\frac{\partial x_j}{\partial t}\right|_M + \left.\frac{\partial u_i}{\partial t}\right|_E \tag{21a}$$

$$\left.\frac{\partial T}{\partial t}\right|_M = \left.\frac{\partial T}{\partial x_j}\frac{\partial x_j}{\partial t}\right|_M + \left.\frac{\partial T}{\partial t}\right|_E \tag{21b}$$

where the subscript M denotes the moving mesh, the subscript E the Eulerian description, and $\partial x_j/\partial t$ is the velocity of the mesh. In the Galerkin formulation, the continuity, momentum, and energy equations in the moving mesh system are

$$\int \Psi\left[\frac{\partial \hat{u}_i}{\partial x_i}\right] dv = 0 \tag{22a}$$

$$\int \rho\Phi\left[\frac{\partial \hat{u}_i}{\partial t} + (\hat{u}_j - U_j^*)\frac{\partial \hat{u}_i}{\partial x_j}\right] dV + \int \sigma_{ij}\frac{\partial \Phi}{\partial x_j} dV - \int \rho g_i \Phi\, dV - \int \Phi\sigma_{ij} n_j\, dA = 0 \tag{22b}$$

$$\int \Theta\rho C_p\left[\frac{\partial T}{\partial t} + (\hat{u}_j - U_j^*)\frac{\partial \hat{T}}{\partial x_j}\right] dV + \int q_j\frac{\partial \Theta}{\partial x_j} dV - \int \Theta q_j n_j\, dA = 0, \tag{22c}$$

where Ψ, Φ, and Θ are the finite element shape functions, and U_j^* is the element convection velocity. When $U_j^* = u_j$, these equations are Lagrangian.

Because of shearing, the moving mesh will become distorted after a few time steps. An efficient remeshing algorithm is needed to reconstruct the mesh to assure the solution quality for continuous computation. Two effective remeshing schemes have been developed and tested [26]: one is convective adjustment and the other is search and interpolation. The basic concept of the convective adjustment scheme is to treat the action of remeshing as an extra nodal movement during that time step, making it equivalent to an additional convection term. Because this convective adjustment term is required for the matrix forming and solution, a complete time step is taken to finish the remeshing. The number of nodes and elements are constant before and after remeshing. In this scheme, the convective term has to be modified to include both the moving mesh and the remeshing effects.

In the search and interpolation scheme, remeshing is considered to be a snapshot without time passage, and the updated Lagrangian formulation is continuously used throughout the computation. The search is to determine where in the old mesh element the new node is located. This can be implemented by checking the cross product between the new nodal vector and the four sides of each element. The unknowns at the new nodes such as velocity and temperature, have to be interpolated from the local coordinates of the old mesh. Both schemes yield the same velocity, pressure, and temperature profiles after remeshing and require almost the same computing time, but the search and interpolation scheme requires more programming effort.

IV. MODELING OF DRAWING PROCESS

To illustrate the procedures involved and the information revealed in modeling, a drawing process will be modeled in this section. In a continuous drawing process, material is melted in an induction heating furnace and the melt is drawn past a mandrel to form a cylindrical tube. The complex interactions between the temperature, flow, and electromagnetic fields prohibit the empirical development of this process. An integrated finite element analysis including all three fields was developed to optimize the process design and the processing conditions.

For continuous forming processes, such as the drawing process considered, the problems are basically steady state and the standard Eulerian coordinates are well suited. The technical challenge here is to locate the free surfaces. Since the solution field is a function of the surface shape which is not known a priori, it becomes a geometrically nonlinear problem. A mathematical description of the free surface has to be defined. An effective way [29] to trace the free surface

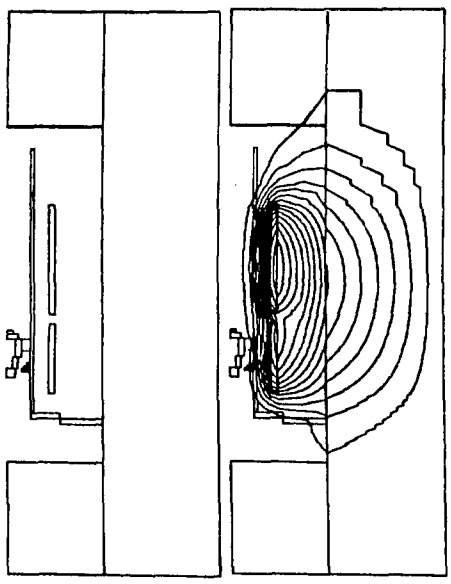

FIG. 1. Computed electromagnetic field of induction furnace.

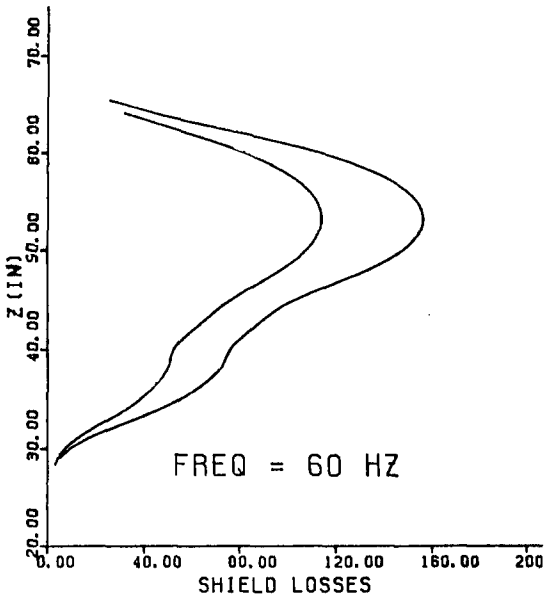

FIG. 2. Computed susceptor shield loss.

is to successively compute the r-coordinates by integrating the streamline equation. The location of the starting node on the free surface, e.g., die exit, is generally known.

The process can be described in the following manner. First, the induction heating coils induce an eddy current on the susceptor, which subsequently generates heat due to Joule heating. The electromagnetic field calculations provide useful insights for the induction coil design through sensitivity analysis of the current density distribution profile [12]. Next, the induced heat is transported from the susceptor to the forming material by thermal conduction, convection, and radiation. The temperature distribution obtained from the thermal analysis is needed to analyze the energy balance, the cooling system, and the structural integrity.

Once the temperature reaches the softening point, the material starts to flow under gravity, assisted by the applied traction (downstream). Since the material viscosity is highly temperature-dependent, the flow rate and the tube dimension (free surface) are very sensitive to the temperature distribution of the furnace, especially near the die exit where most of the shear stresses occur. A finite element viscous flow model with steady-state free surface tracking capability is needed for analyzing the parametric relationships.

Since the tube drawing process is continuous, a steady-state assumption is applied in both the flow and temperature calculations. For analyzing the induced eddy-current distribution generated by the induction coils inside the furnace, the following assumptions were made [12]: (1) it is an axisymmetric field represented by a single-component vector potential which is perpendicular to the cross section; (2) the eddy-current regions, i.e., the susceptor and the metallic structure parts, are source-free, and the source current is also free of eddy current; and (3) the vector potential and the source current are harmonic functions of time while the magnetic permeability is field-independent.

Figure 1 shows a typical contour plot of the magnetic field of the furnace; Fig. 2 gives the axial distribution of the calculated susceptor shield loss, which is treated as the heat source in the heat transfer analysis of the furnace. The computational domain of the electromagnetic field is much larger than the physical furnace size because of a more realistic boundary condition. Both the boosting mode and the bucking mode of the coil design were numerically tested under various frequencies.

Because the optical thickens of thermal radiation is smaller than the furnace dimension, the diffusion approximation with an effective thermal conductivity is appropriate. The Rosseland mean absorption coefficient was integrated over the wavelength band using the fractional function of the second kind [12, 25]. The computed temperature profiles, as shown in Fig. 3, are in good agreement with the measured data.

The flow analysis gives the profiles of velocity and pressure and the free surfaces, i.e., the inside and outside diameters of the drawn tube. Figure 4 shows the calculated streamlines of the furnace under certain operating condi-

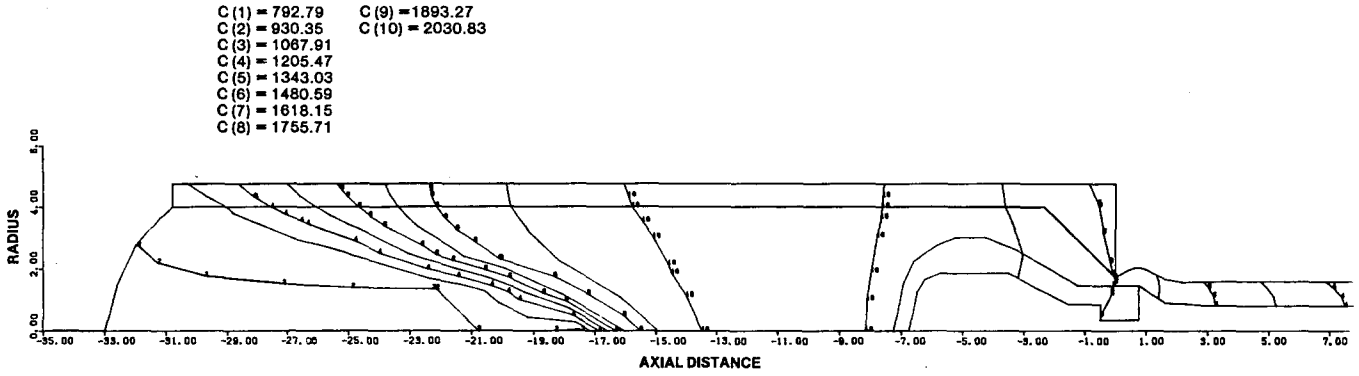

FIG. 3. Computed temperature contours.

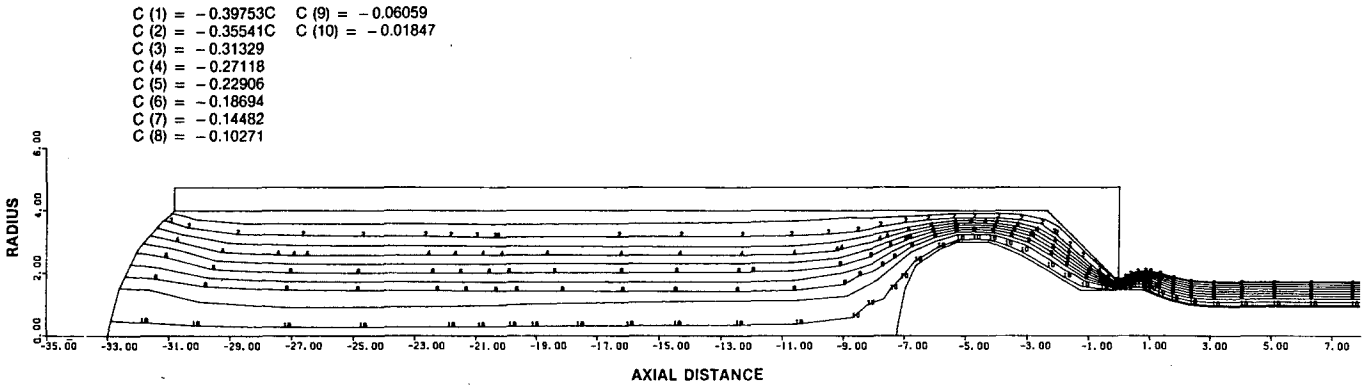

FIG. 4. Computed streamlines.

tions. The correlations among the mandrel/die geometry, draw speed, ambient environment, and tube dimensions are all important factors in the process design. This integrated finite element system is indeed a powerful engineering analysis tool, which can help optimize the processing condi-

Nucleation

Nucleation is a very important phenomenon in material processing. In this subsection, the modeling of nucleation of grains during solidification and recrystallization is reviewed.

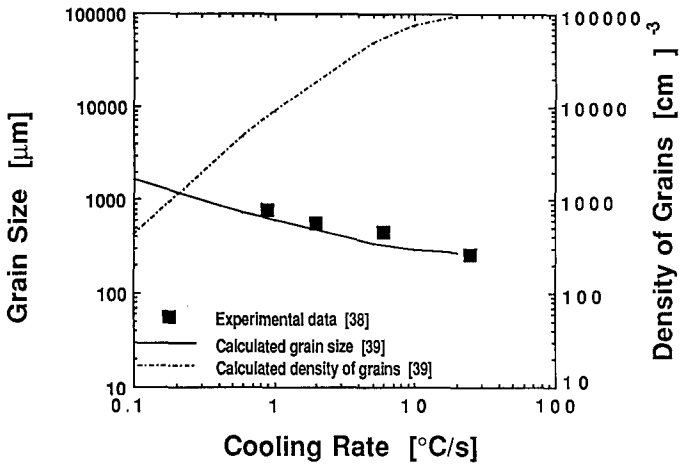

FIG. 5. Variation of grain size and grain density with cooling rate.

instant nucleation model [42] are used to describe nucleation during recrystallization. Since this instant nucleation model is almost a delta function, it requires a small time step for obtaining accurate results.

Growth of Grains during Solidification

The kinetics of the growth of grains is governed by the volume diffusion of solute and the interface curvature of the grain, which can be expressed by Fick's law and the Poisson equation. During solidification, the volume diffusion of solute in the liquid is the dominant factor of the growth kinetics. The growth rate of the dendrite, or eutectic phase, v, at a given undercooling, ΔT, can be carried out by solving the diffusion equation [43–46] and by using the surface instability theory [47, 48]. For both dendrite and eutectic solidification, the grain growth rate can be approximately expressed as a polynomial expression of undercooling. In addition, the nucleation may occur simultaneously during the growth process. The coupled nucleation–growth process needs a more restrictive time step during simulation to obtain convergent results.

Growth of Grains during Recrystallization

During recrystallization (also known as Ostwald ripening), the growth of grains is governed by the surface energy characterized by the interface curvature of the grains rather than the volume diffusion of mass. This process is referred to as the "multiparticle diffusion problem," as shown in Fig. 6a, where the location of particles in space is random. This problem can be described by the Poisson equation,

$$\frac{\partial^2\theta}{\partial x_i^2} = \sum_{j=1}^{N} -4\pi\beta_j\delta(r_i - r_i^j), \tag{23}$$

where N is the number of sources and sinks in the system, r_i and r_i^j are the dimensionless vectors locating the arbitrary

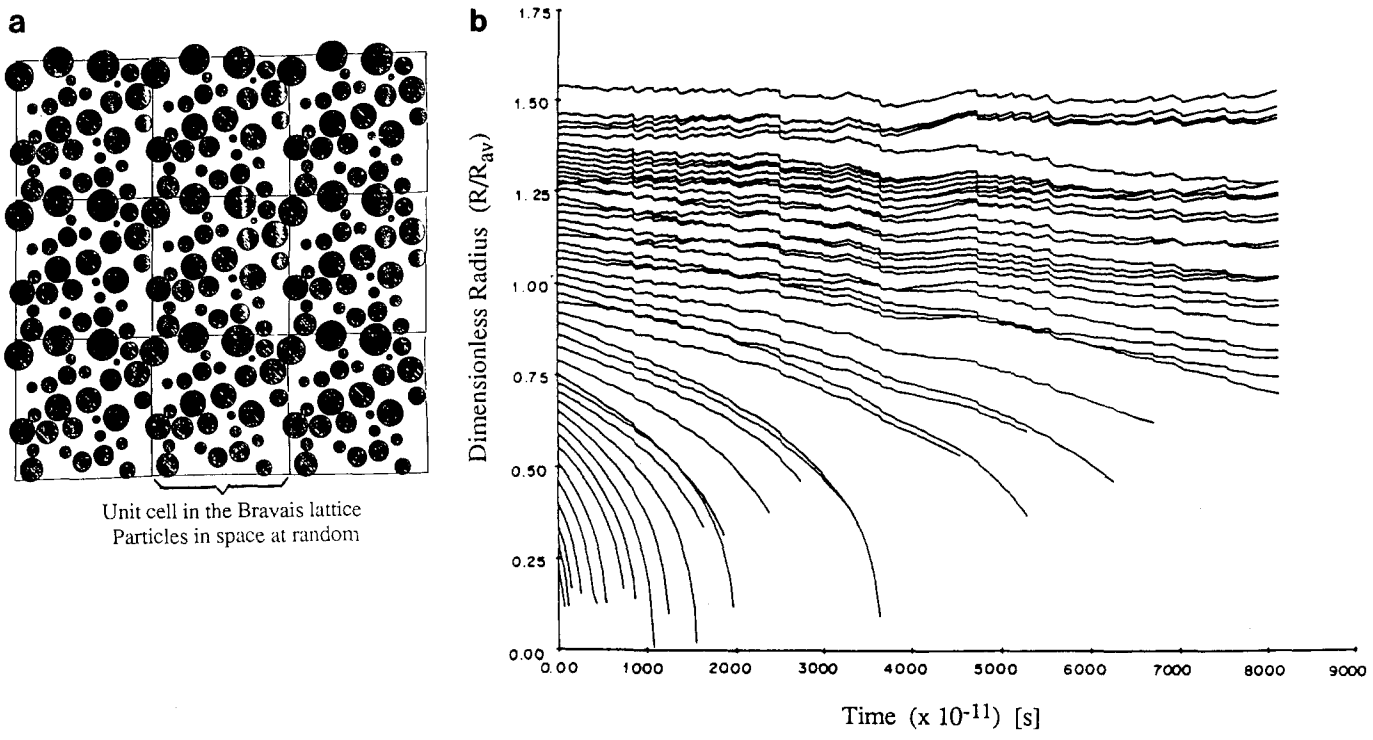

FIG. 6. Grain size and its evolution [50].

field point and the jth source or sink, β_i is the strength of the ith source or sink, and θ is the dimensionless temperature, pressure, solute concentration, etc.

The Poisson equation can be solved by the method of potential theory. A general solution to the Poisson equation is the linear combination

$$\theta(r_i) = \beta_0 + \sum_{j=1}^{N} \frac{\beta_j}{|r_i - r_i^j|}, \tag{24}$$

where β_0 is some constant reference potential which, in general, is nonzero. The β_j series will converge only under the condition [49]

$$\lim_{N \to \infty} \sum_{j=1}^{N} \beta_j = 0. \tag{25}$$

If a spatial location of the particles may be specified through the use of a periodic arrangement such as the Bravais lattice and a unit cell in which the location of the particles in space is at random, the above equation can be reformulated into a rapidly convergent series. The Bravais lattice provides the overall spatial periodity, whereas the unit cell provides the spatial randomness necessary to model stochastic multiparticle diffusion [49, 50].

When the location of particles in space obeys the above arrangement, the growth rate of grains, dR_i/dt, can be calculated by applying the boundary conditions, $\theta_j = -1/R_j$, to the multiparticles diffusion solution,

$$\frac{dR_i}{dt} = \frac{\beta_i}{R_i^2}, \qquad i = 1, 2, ..., N \tag{26}$$

and β_i can be derived by the set of linear equations,

$$Y_j = \chi_{ij} \beta_j, \tag{27}$$

where

$$Y_j = \begin{cases} 0, & j = 0, \\ -1/R_j, & j = 1, N, \end{cases} \qquad \beta_j, j = 0, N,$$

where β_j is the sink strength, and the coefficient matrix, χ_{ij}, is expressible in symmetric form. When the volume fraction tends toward zero, i.e., $f \to 0$, a particularly simple form of the coefficient matrix can be obtained:

$$\chi_{ij} = \begin{bmatrix} R_1^{-1} & 0 & 0 & \cdots & 1 \\ 0 & R_2^{-1} & 0 & 0 & \cdots & 1 \\ \cdots & \cdots & \cdots & \cdots & \cdots & \cdots \\ \cdots & \cdots & \cdots & \cdots & \cdots & \cdots \\ 1 & 1 & 1 & & & 0 \end{bmatrix}.$$

The calculated grain size evolution as a function of time is shown in Fig. 6b [50] at a volume fraction of $f = 0.35$. According to this solution, the smallest grains dissolve quickly, the grains with medium size grow at the beginning and shrink after a certain time, and the biggest grains continue to grow gradually. This method can obtain a relatively stable and convergent solution for a large range of time steps, but it requires that the number of particles must be large enough to obtain the approximate stochastic distribution of grains in the space, e.g., more than 3000 particles. The simulation with so large a number of particles is, of course, computationally intensive.

Although the matrix method can provide a relatively quick solution, it requires several restrictions, such as: the particles must be spherical, no secondary phase particles exist, etc. In this case, the Monte Carlo method is applied to simulate grain growth during the recrystallization process [51–53]. The Monte Carlo method for solving a deterministic problem such as grain recrystallization is performing an experiment in which each particle movement is considered as a random process until it is absorbed on a barrier (e.g., the grain boundary). This method can provide a more accurate microstructure with various grain morphologies and converge at a much larger range of conditions, such as the presence of secondary phase particles, anisotropic grain boundary energies, and abnormal grain growth. However, it is worth noting that the convergence of the Monte Carlo method is usually slower than that of the matrix calculation. In addition, the Monte Carlo method needs to calculate the movements of more than 40,000 particles [50] to perform the microstructure evolution.

When using the Monte Carlo method, a continuum microstructure is mapped onto a discrete lattice containing a large number of lattice sites, N (Fig. 7). Each lattice site is assigned a number between 1 and Q which corresponds to the orientation of the grain in which it is embedded. Lattice sites which are adjacent to neighboring sites having different grain orientations are regarded as the grain boundary while sites surrounded by the same grain orientation are the grain

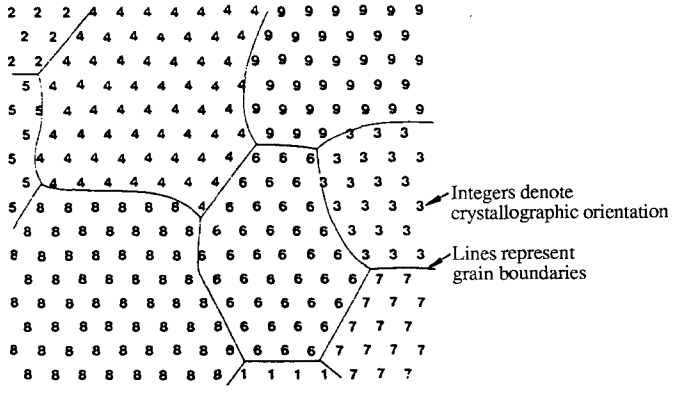

FIG. 7. Sample microstructure on a triangular lattice [51].

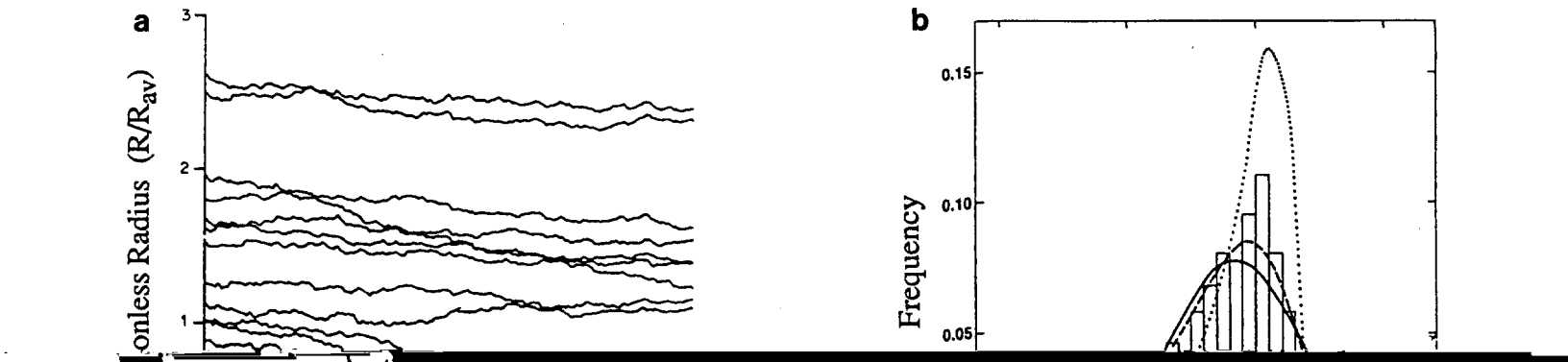
a
onless Radius (R/R$_{av}$)
3
2
1
b
Frequency
0.15
0.10
0.05

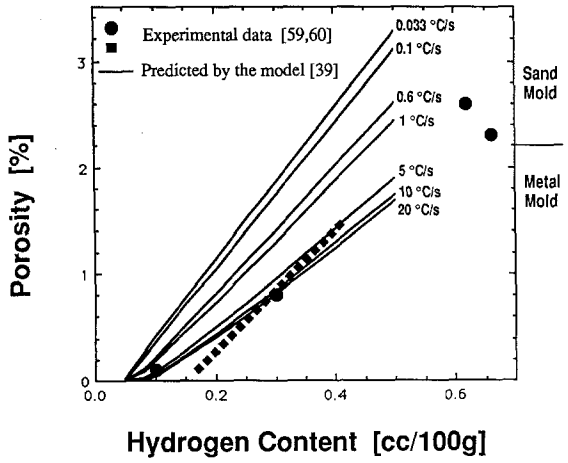

FIG. 10. Amount of porosity as a function of gas content and cooling rate.

prediction of the Monte Carlo method is closer to measured grain size distribution [52].

When secondary phase particles are present, they are incorporated into the model by making their orientations different than those of the primary sites. In this way, the particles–matrix interface has the same energy as the grain boundary. By using the above assumptions, a 3D microstructure evolution as a function of time at a given volume fraction, $f = 0.01$, is shown in Fig. 9.

Defect Formation

Since the final properties of materials depend strongly on defects in those materials, defect formation has received significant attention in modeling of material production processes. Among other defects, porosity (or voids) in castings or other materials is considered the major defect which impairs the mechanical properties and service life of materials. Most porosity forms during the cooling or solidification processes. During solidification, the fraction solid increases with the cooling of the material. When the solid–liquid interface advances toward bulk liquid, the gas dissolved in the melt is rejected at the interface because the solid phase exhibits an extremely low solubility in gas. Consequently, the gas concentration in the bulk liquid increases with fraction solid until pores form. Simultaneously, when the liquid phase transforms to the solid phase and cools from a high temperature to a low one, volume contraction occurs. This is referred to as "shrinkage." The coupled effect of gas enrichment in the liquid and shrinkage at the solid–liquid interface is the major origin of porosity formation [38, 39].

The enrichment of gas in the liquid can be described by the Brody–Flemings equation as indicated by Fang and Granger [38]. Once the pores form, the variation of pore volume fraction can be evaluated by using a general mass balance equation. Zou *et al.* [39] have developed a mathematical model to describe the nucleation and growth of pores. Their model permits the prediction of the pore formation as regards to pore size, pore distribution, and amount of porosity in the castings. The calculated and measured amounts of porosity are presented in Fig. 10 [59, 60].

VI. MACRO/MICROSCOPIC MODELING

As discussed in the previous section on modeling of macroscopic behavior, most macroscopic equations can be solved by the finite difference method or finite element method. The formulation of the macroscopic finite difference or finite element equation is often written as a linear funtion. However, the equations in modeling microstructure, such as the nucleation, growth, and impingement equations are highly nonlinear. In this case, several techniques have been developed to optimize the coupled macro/microscopic modeling process.

There are two types of macro/microscopic modeling: (a) placing microscopic models into macroscopic models and (b) applying the general macroscopic equation to the microstructure scale. When placing the microscopic models into macroscopic models to predict microstructure evolution, the validity of the assumptions used in the microscopic model and nonlinearity of most microscopic models have to accounted for. When applying the macroscopic model to the microstructure scale in such cases as interdentritic fluid flow, filtration, and porosity formation, an average method

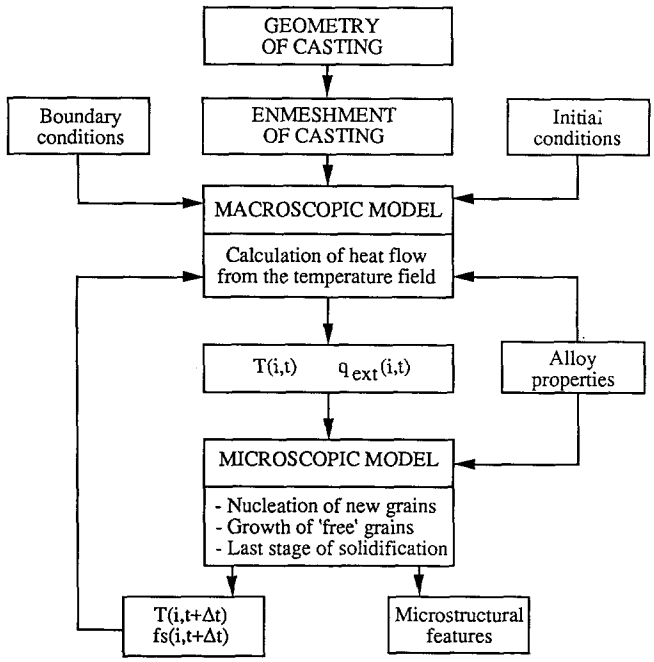

FIG. 11. Flow chart of the macro/microscopic approach for solidification.

is most often used to overcome the difficulty imposed by the complex microscopic geometry.

A schematic representation of the heat transfer macro/microscopic modeling process is illustrated in Fig. 11 [31]. The macroscopic part of the model is used essentially to enmesh the volume to be simulated and then to calculate the heat flow, $q_{ext}(i, t)$, going out of each mesh from the temperature, $T(i, t)$, or variation of the enthalpy at each node (i). Two basic methods were applied to incorporate microscopic models into a macroscopic model: (a) a directly coupled macro–micro scheme called the latent heat method (Fig. 12a) [34]; and (b) a decoupled macro–micro scheme called microenthalpy (Fig. 12b) [58]. The first approach is fully explicit in time and the second approach is fully implicit in time. Since the micromodels are highly nonlinear functions, the stability and convergency of numerical solutions emerge when they are incorporated into the macromodels which are essentially a set of linear functions. In addition, when placing micromodels into macromodels the assumptions made for the microscopic models may not be available for the macroscopic model. However, the finite difference method or some other numerical method allows these assumptions to still be valid in the scale of mesh size in which the micromodels are applied.

The first method directly incorporates the microscopic models into the macroscopic model at each time step. The temperatures calculated from the macromodel are used to evaluate the microstructure evolution which is described by the micromodels. Then, the variation of fraction solid calculated from the micromodels is fed directly back into the next time step of macroscopic calculation. The advantage of this method is in obtaining an accurate solution. It is found [34] that the numerical solution converges primarily with smaller mesh size rather than smaller time step. As a result,

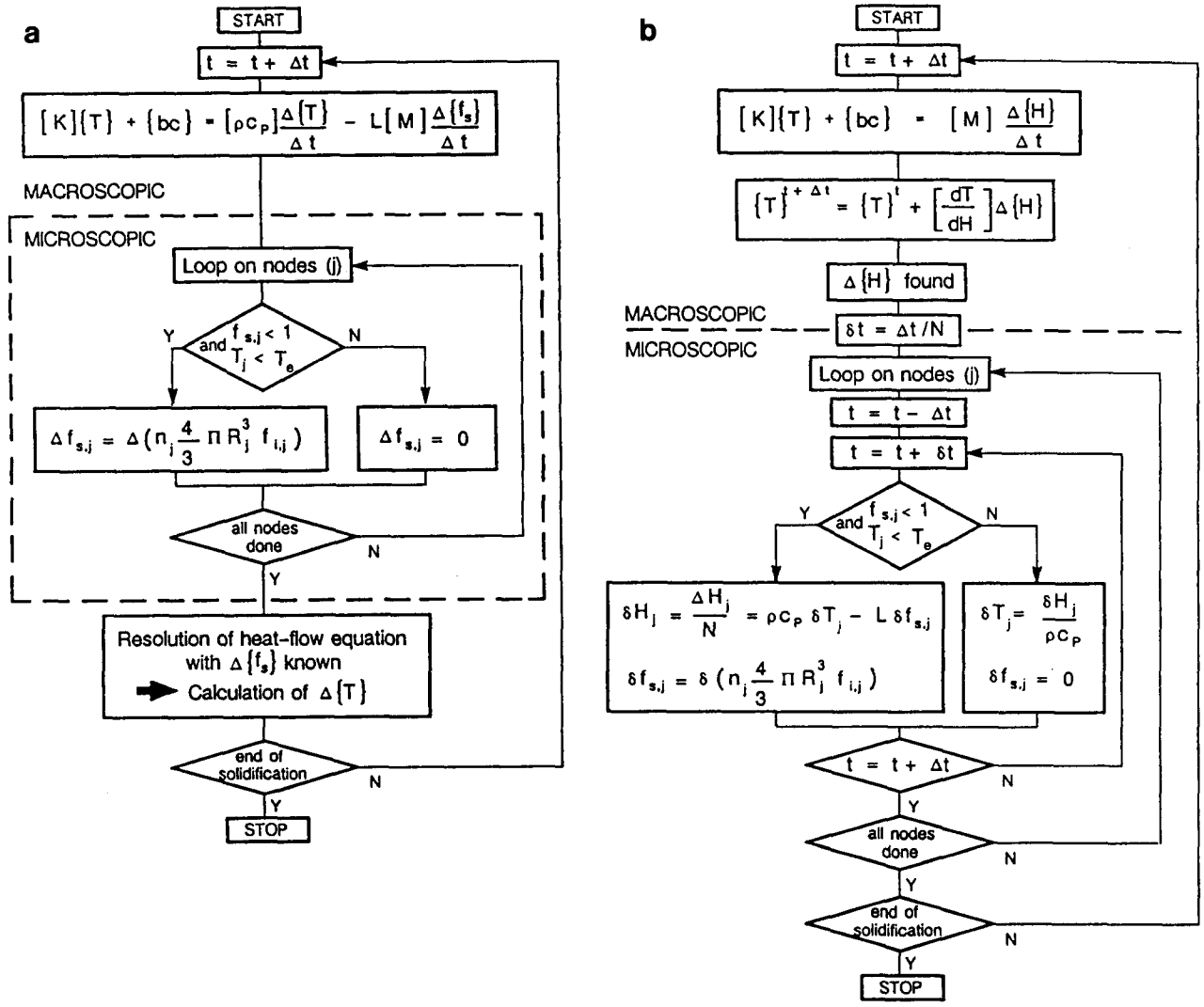

FIG. 12. Flow chart of two coupling schemes between macro and micromodeling.

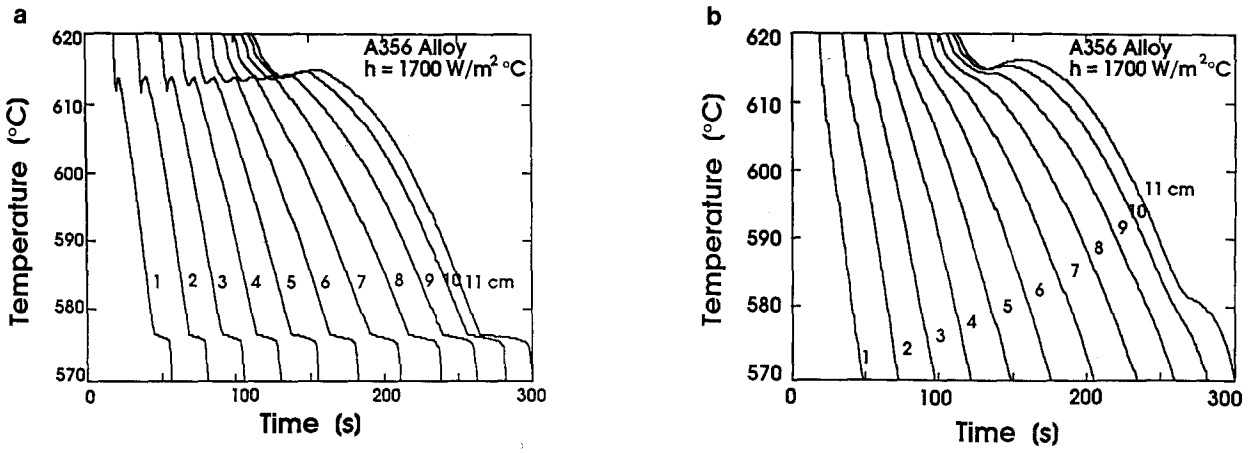

FIG. 13. Microscopic and macroscopic temperature evolutions during solidification.

to gain an accurate solution by adopting a finer mesh size leads to a larger number of meshes in the 2D and 3D simulations. This is the major disadvantage of this method.

The decoupled macro–micro method developed by Thevoz *et al.* [58] separates the microscopic calculation from the macroscopic calculation. The macroscopic calculation has been performed by the standard enthalpy method without feedback from the microscopic model. A much smaller microscopic time step has been proposed, e.g., $\Delta_{tmic} = \Delta_{tmac}/100$ to obtain stable and convergent macro–micro results. In this case, a larger macroscopic time step obtain a stable microstructure evolution through the separated microscopic calculations and to determine the accurate macroscopic heat flow by feeding the variation of fraction solid directly back to the macroscopic heat flow calculation. Consequently, a more accurate solution than that of Thevoz *et al*'s can be expected. Meanwhile, this method retains all the merits of the previous method. An example of the macro/microscopic calculation of temperature evolution is shown in Fig. 13.

VII. CONCLUDING REMARKS

methods. Although finite difference methods today are not as popular as they once had been, some well-proven programs are still widely used [1, 2, 61, 62] and new schemes are continuously being developed [4, 6–8, 63]. During the past 15 years, finite element methods have become a common tool for modeling material processing [64]. More recently, boundary element methods have appeared as a promising alternative approach [65, 66].

Owing to rapid developments in the microprocessor field during recent years, personal computers with sufficient capacity to perform finite element and finite difference calculations are now available, while advances in software have allowed a user-friendly interface to be provided [67]. It is expected that the artificial intelligence or expert system techniques will be incorporated into the modeling process, especially in the areas of mesh generation and result interpretation [4, 68, 69].

As computer capacity increases and the cost of computation decreases, it is to be expected that more and more three-dimensional problems will be attempted. A major stumbling block is the difficulty of interpreting the results. In two-dimensional analyses, graphical displays of meshes or results are considered almost essential. For three-dimensional problems, graphical displays of results or input are considered even more essential [30, 61]. Unfortunately, the three-dimensional representation of three-component vector fields in an easily interpretable and comprehensible fashion is still an unsolved problem. Hence the cost of three-dimensional solutions will, for the foreseeable future, remain high in terms of human labor, even though the computational cost is decreasing rapidly.

APPENDIX: NOMENCLATURE

a	constant
A_i	vector field, $\partial A_k/\partial x_i = B_i$
b_i	body force, N
B_i	magnetic-flux density
C_p	specific heat capacity, $J/m^3 - K$
C_{ijk}	third-order tensor resistance coefficient
e_{ijk}	permutation symbol
E_i	electric-field intensity
f	volume fraction
F	emissive-geometric factor
g_i	gravitation, m/s^2
G	lattice site energy, J
h_c	heat transfer coefficient, $W/m^2 - K$
H	magnetic-field intensity
J	current density
k	thermal conductivity, $W/m - K$
k_B	Boltzman constant, J/K
K	consistency index or permeability, m^2
L	heat of fusion per volume, J/m^3
m	boundary mobility, m/s
n	flow index
nn	nearest neighbor sites
N	number of sources and sinks in the system
p	pressure, N/m^2
q	heat flux, W/m^2
Q	a large number
r_i	dimensionless location vectors
R	radius of grains, m
S	surface tension coefficient or surface, m^2
t	time, s
T	temperature, K or $^\circ C$
u_i	velocity vectors, m/s
U_j^*	element convection velocity, m/s
W	transition probability
x_i	Cartesian coordinates, m
Y_j	negative curvature of grain interface, $-1/R_j, m^{-1}$
β_i	sink strength, m^3/s
γ_{ij}	rate-of-tensor
δ_{ij}	Kronecker delta
η	apparent viscosity, m^2/s
η_m	magnetic permeability
θ	dimensionless temperature, pressure, solute concentration, etc
μ	viscosity, $N - s/m^2$
μ_m	magnetic permeability
ρ	density of materials, kg/m^3
ρ_1, ρ_2	principal radii of curvature of surface, m^{-1}
σ_e	electric conductivity
σ_{ij}	stress tensor
σ_{SB}	Stefan-Boltzman constant, $W/m^2 - K^4$
ϕ	dissipation function
Ψ, Φ, Θ	finite element shape function
χ	coefficient matrix
$\partial x_j/\partial t$	velocity of the mesh, m/s

Subscripts

ext	at the interface
E	Eulerian description
i, j, k	coordinate index
l	liquid or liquidus
mac	macroscopic
mic	microscopic
M	moving mesh
r	radiative
s	solid or solidus
∞	ambient state

ACKNOWLEDGMENTS

The authors are grateful to the National Science Foundation under Grant No. DDM-8912345 and Occidental Chemical Corp for their support of this work. Acknowledgments are also due to Dr. J. J. M. Too of Energy, Mines and Resources Canada, Ottawa, Canada, for his valuable suggestions.

REFERENCES

1. A. A. Tseng, D. R. Durham, and R. Komanduri (Eds.), *Manufacturing Simulation and Processes*, PEDO, Vol. 20 (Am. Soc. Mech. Eng., New York, 1986).
2. A. A. Tseng (Ed.), *Modeling of Materials Processing*, MD, Vol. 3 (Am. Soc. Mech. Eng., New York, 1987).
3. F. Rodriguez, *Principle of Polymer Systems*, 2nd ed. (Hemisphere, Washington, DC, 1982).
4. A. A. Tseng and J. C. Cheng, *J. Eng. Mater. Technol.* **113**, 384 (1991).
5. S. V. Patankar, *Numerical Heat Transfer and Fluid Flow* (McGraw–Hill, New York, 1980).
6. A. A. Tseng, *Int. J. Numer. Methods Eng.* **20**, 1885 (1984).
7. A. A. Tseng and P. F. Sun, *Int. Polym. Process.* **5**, 292, 1990.
8. S. V. Patankar and D. B. Spalding, *Int. J. Heat Mass Transfer* **15**, 1787 (1972).
9. Y. A. S. Aregbesola and D. M. Burley, *J. Comput. Phys.* **24**, 398 (1977).
10. S. Genesan and D. R. Poirier, *Metall. Trans. B* **21**, 173 (1990).
11. N. Shamsunder and E. M. Sparrow, *J. Heat Transfer* **97**, 333 (1975).
12. A. A. Tseng, *Adv. Eng. Software* **10**, 58 (1988).
13. R. E. Nickell, I. Tanner, and B. Caswell, *J. Fluid Mech.* **65**, 189 (1974).
14. P. W. Chang, T. W. Patten, and B. Finlayson, *Comput. Fluids* **7**, 285 (1979).
15. S. F. Kistler and L. E. Scriven, in *Computational Analysis of Polymer Processing*, edited by J. R. A. Pearson and S. M. Richardson (Appl. Sci., New York, 1983).
16. R. I. Tanne, in *Computational Analysis of Polymer Processing*, edited by J. R. A. Pearson and S. M. Richardson (Appl. Sci., New York, 1983).
17. K. R. Reddy and R. I. Tanner, *Comput. Fluids* **6**, 83 (1978).
18. F. M. Orr and L. E. Scriven, *J. Fluid Mech.* **84**, 145 (1978).
19. G. Ryskin and L. G. Leal, *J. Fluid Mech.* **148**, 1 (1984).
20. K. J. Ruschak, *Int. J. Numer. Methods Eng.* **15**, 639 (1980).
21. B. A. Finlayson, *The Method of Weighted Residuals and Variational Principles* (Academic Press, New York, 1972).
22. P. Bach and O. Hassager, *J. Fluid Mech.* **152**, 173 (1985).
23. Z. Tadmor, E. Broyer, and C. Gutfiger, *Polym. Eng. Sci.* **14**, 660 (1974).
24. C. W. Hirt, A. A. Amsden, and J. L. Cook, *J. Comput. Phys.* **14**, 227 (1974).
25. C. W. Hirt and B. D. Nichols, *J. Comput. Phys.* **39**, 201 (1981).
26. H. P. Wang and R. T. McLay, in *Proceedings, Fifth International Symposium on Finite Elements and Flow Problems*, edited by J. T. Oden (Texas Institute of Computational Mechanical, Austin, TX, 1984), p. 521.
27. H. P. Wang, in *Computer Integrated Manufacturing and Robotics*, edited by M. Leu, PED, Vol. 13 (ASME, New York, 1985), p. 361.
28. H. P. Wang and R. T. McLay, *J. Fluid Eng.* **108**, 465 (1986).
29. I. Tanner, R. E. Nickell, and R. W. Bilger, *Comput. Methods Appl. Mech. Eng.* **6**, 155 (1975).
30. S. R. H. Hoole, *The Computer Aided Analysis and Design of Electromagnetic Devices* (Elsevier, New York, 1989).
31. M. Rappaz, Ph. Thévoz, J. Zou, J.-P. Gabathuler, and H. Lindschied, in *State of the Art of Computer Simulation of Casting and Solidification Processes*, edited by H. Fredriksson (E-MRS, Strasbourg, France, 1986), p. 277.
32. M. Rappaz and Ph. Thévoz, *Acta Metall.* **35**, 1487 (1987).
33. W. Brostow, *Science of Materials* (Krieger, Melbourne, FL, 1985).
34. J. Zou and A. A. Tseng, *Metall. Trans. A* **23**, 457 (1992).
35. K. C. Su, I. Ohnaka, I. Yamauchi, and T. Fukusako, *Mat. Res. Soc. Symp. Proc.* **34**, 181 (1985).
36. D. M. Stefanescu and C. Kanetkar, in *Computer Simulation of Microstructure Evolution*, edited by D. J. Srolovitz (TMS-AIME, Warrendale, PA, 1986), p. 171.
37. I. Maxwell and A. Hellawell, *Acta Metall.* **23**, 229 (1975).
38. Q. T. Fang and D. A. Granger, *AFS Trans.* **97** (1989).
39. J. Zou, S. Shivkumar, and D. Apelian, *AFS Trans.* **99**, 87 (1989).
40. W. A. Johnson and R. F. Mehl, *Trans. Am. Inst. Min. Eng.* **135**, 146 (1939).
41. M. Avrami, *J. Chem. Phys.* **7**, 1103 (1939); **8**, 212 (1940); **9**, 177 (1941).
42. T. O. Saetre, O. Hunderi, and E. Nes, *Acta Metall.* **34**, 981 (1986).
43. K. A. Jackson and J. D. Hunt, *Trans. Metall. Soc. AIME* **236**, 1129 (1966).
44. W. Kurz and D. J. Fisher, *Fundamentals of Solidification* (Trans. Tech. Pub., Aedermannsdorf, Switzerland, 1986).
45. W. Kurz and R. Trivedi, *Acta Metall.* **38**, 1 (1990).
46. J. D. Hunt, *Mat. Sci. Eng.* **65**, 75 (1984).
47. W. W. Mullins and R. F. Sekerka, *J. Appl. Phys.* **35**, 444 (1964).
48. J. S. Langer and H. Müller-Krumbhaar, *J. Cryst. Growth* **42**, 11 (1977).
49. P. W. Voorhees and M. E. Glicksman, *Acta Metall.* **32**, 2001 (1984).
50. P. W. Voorhees and M. E. Glicksman, *Acta Metall.* **32**, 2013 (1984).
51. M. P. Anderson, D. J. Srolovitz, G. S. Grest, and P. S. Sahni, *Acta Metall.* **32**, 783 (1984).
52. D. J. Srolovitz, M. P. Anderson, P. S. Sahni, and G. S. Grest, *Acta Metall.* **32**, 793 (1984).
53. M. P. Anderson, G. S. Grest, R. D. Doherty, K. Li, and D. J. Srolovitz, *Scripta Metall.* **23**, 735 (1989).
54. P. Feltham, *Acta Metall.* **5**, 97 (1975).
55. M. Hillert, *Acta Metall.* **13**, 227 (1965).
56. N. P. Louat, *Acta Metall.* **22**, 721 (1974).
57. M. Rappaz, *Inter. Mater. Rev.* **34**, 93 (1989).
58. Ph. Thévoz, J. L. Desbiolles, and M. Rappaz, in *Modeling of Casting and Welding Processes IV* (TMS, Palm Coast, FL, 1988).
59. R. A. Entwistle, J. E. Gruzleski, and P. M. Thomas, in *Solidification and Casting of Metals*, (Metals Soc., London, 1977), p. 345.
60. B. R. Deoras and V. Kondic, *Foundry Trade J.* **100**, 361 (1956).
61. R. M. Lueptow, *Computers in Mechanical Engineering* **March/April**, 10 (1988).
62. W. Muller, J. Krueger, A. Jacobus, R. Winz, T. Weiland, H Euler, U. Hamm, and W. R. Novender, *Archi. Electrotech. (Berlin)* **65**, 299 (1982).
63. W. Muller, *IEEE Trans. Magn.* **MAG-18**, 588 (1982).
64. O. C. Zienkiewicz, *The Finite Element Method*, 3rd ed. (McGraw–Hill, New York, 1977).
65. P. K. Banerjee and R. Butterfield, *Boundary Element Methods in Engineering Science* (McGraw–Hill, London, 1981).
66. G. Meunier, J. L. Coulomb, S. J. Salon, and L. Krahenbul, *IEEE Trans. Magn.* **MAG-22**, 1040 (1986).
67. M. Kalwa, in *Proceedings of ANTEC'88, 46th Annual Technical Conference of SPE, 1988*, p. 1771.
68. J. L. Chen and P. Hajela, *Comput. Struct.* **29**, 99 (1988).
69. M. F. Russo, R. L. Peskin, and Kowalski, A. D., *Simulation* **49**, 150 (1987).